Available online at www.sciencedirect.com
SCIENCE DIRECT
Polymer 46 (2005) 3906–3913
polymer
www.elsevier.com/locate/polymer

Segregation morphology of poly(3-hydroxybutyrate)/poly(vinyl acetate) and poly(3-hydroxybutyrate-*co*-10% 3-hydroxyvalerate)/poly(vinyl acetate) blends as studied via small angle X-ray scattering

Hsiu-Jung Chiu*

Department of Chemical and Materials Engineering, Ta Hwa Institute of Technology, 1, TaHwa Road, Chiunglin, Hsinchu 30703, Taiwan, ROC

Received 20 July 2004; received in revised form 2 January 2005; accepted 11 March 2005
Available online 2 April 2005

Abstract

Segregation morphology of poly(3-hydroxybutyrate) (PHB)/poly(vinyl acetate) (PVAc) and poly(3-hydroxybutyrate-*co*-10% 3-hydroxyvalerate) (P(HB-*co*-10% HV)/PVAc blends crystallized at 70 °C have been investigated by means of small angle X-ray scattering (SAXS). Morphological parameters including the crystal thickness (l_c) and the amorphous layer thickness (l_a) were deduced from the one-dimensional correlation function ($\gamma(z)$). Blending with PVAc thickened the PHB crystals but not the P(HB-*co*-10% HV) crystals. On the basis of the composition variation of l_a, and the volume fraction of lamellar stacks (ϕ_s) revealed that PHB/PVAc blends created the interlamellar segregation morphology when the weight fraction of PVAc (w_{PVAc}) ≤ 0.2 and the interlamellar and interfibrillar segregation coexisted when $w_{PVAc} > 0.2$, while P(HB-*co*-10% HV)/PVAc blends yielded the interfibrillar segregation morphology at all blend compositions. For both PHB/PVAc and P(HB-*co*-10% HV)/PVAc blends, the distance of PVAc segregation was promoted by increasing PVAc composition and the distance of PVAc segregation in P(HB-*co*-10% HV)/PVAc blends was greater than in PHB/PVAc at a given PVAc composition. The crystal growth rate played a key role in controlling the segregation of PVAc.

Keywords: Poly(3-hydroxybutyrate); Poly(3-hydroxybutyrate-*co*-10% 3-hydroxyvalerate); Small angle X-ray scattering

1. Introduction

Binary polymer blends can be classified into amorphous/amorphous, crystalline/amorphous, and crystalline/crystalline systems based on the crystallizability of the constituents. For the latter two systems, where at least one component is crystallizable, the occurrence of liquid–solid phase separation can generate a wide variety of morphological patterns [1]. In a melt-miscible crystalline/amorphous blend, for example, crystallization is accompanied by the segregation of the amorphous diluent. The morphological structure is characterized by the distance over which the diluent is segregated, where the diluent may be expelled into interlamellar, interfibrillar, or interspherulitic regions. These morphological patterns represent the diluent dispersion from the nanoscopic scale to the micrometer scale. Different scales of dispersion may lead to different properties.

Bacterially synthesized poly(3-hydroxybutyrate) (PHB) [2–5] and its co-polymer with 3-hydroxyvalerate (i.e. P(HB-*co*-HV)) [6–8] with biodegradability and biocompatibility characteristics are crystalline polymers. They are attractive for environmental waste management when used in specific applications. They are naturally occurring and harmlessly biodegradable to water and carbon dioxide by a wide variety of bacteria. P(HB-*co*-HV) co-polymer is one of the most important co-polymers of PHB family. P(HB-*co*-HV) co-polymers being crystallized in either the HB unit cell or the HV unit cell exhibit the unusual phenomenon of co-crystallization and isodimorphism [9–12]. The transformation from the HB lattice to the HV lattice occurred at about 30 mol% HV. Yoshie et al. [13] have studied the structure of the isomorphous crystals of P(HB-*co*-HV) in the PHB crystalline lattice. It has been shown that the composition dependence of spherulitic growth rate, crystallinity, lamella thickness, HV content in the crystalline phase and melting

* Tel.: +886 359 235 51; fax: +886 359 273 10.
E-mail address: hjc@thit.edu.tw.

0032-3861/$ - see front matter © 2005 Elsevier Ltd. All rights reserved.
doi:10.1016/j.polymer.2005.03.032

temperature varied discontinuously at ca. 10 mol% HV, suggesting that a structure transition occurred at ca. 10 mol% HV. Yoshie et al. [13] have introduced two models of lamellar crystals containing co-units, i.e. sandwich lamella model and uniform lamella model, and concluded the crystalline structures formed for HV content below and above 10 mol% can be described by the sandwich lamella model and the uniform lamella model, respectively.

Small-angle X-ray scattering (SAXS) is a very powerful tool for probing the detailed microstructure of crystalline/amorphous blends. By utilizing the SAXS technique, the lamellar morphology of PHB/poly(methyl methacrylate) (PMMA) [14], PHB/poly(vinyl acetate) (PVAc) [15] blends, P(HB-*co*-10% HV)/PMMA blends [16,17] have been studied. For the PHB/PMMA blends, Canetti et al. [14] reported that the higher glass transition temperature (T_g) PMMA was completely segregated into the PHB interlamellar regions (i.e. interlamellar morphology). The P(HB-*co*-10% HV)/PMMA blends mainly generated the interfibrillar segregation morphology at studied crystallization temperatures (i.e. $T_c = 28$–110 °C). For PHB/PVAc blends, it was found that when PVAc composition $w \leq 20$ wt%, the morphology was predominantly characterized by the interlamellar segregation; above this composition, interlamellar and interfibrillar segregation coexisted and the extent of interfibrillar segregation increased with the increase of crystallization temperature (i.e. $T_c = 70$–125 °C).

In the present study, we examine the effect of HV comonomer units on the segregation behavior of PVAc in the PHB-based blends. It will be shown that P(HB-*co*-10% HV)/PVAc blends exhibiting a slower crystal growth rate than the corresponding PHB/PVAc blends display a larger extent of interfibrillar segregation. The further supports the postulate that crystal growth rate plays a crucial role governing the segregation distance of the amorphous diluent in crystalline/amorphous blends.

2. Experimental

2.1. Materials and sample preparation

PHB with $M_n = 2.93 \times 10^5$ and $M_w = 6.5 \times 10^5$, and PVAc with $M_w = 8.3 \times 10^4$ was purchased from Aldrich Chemical Co. The random P(HB-*co*-10% HV) co-polymer containing 10 mol% HV content ($M_n = 1.41 \times 10^5$ and $M_w = 2.13 \times 10^5$) was purchased from Fluka Chemical Co., respectively. PHB and P(HB-*co*-10% HV), respectively, were blended with PVAc by solution casting. The blending components were dissolved in DMF at room temperature yielding a 1 wt% solution. The solution was subsequently poured onto a Petri dish and the blend film was obtained after evaporating most of the solvent on a hot plate at ca. 90 °C. The blend film was further dried in a vacuum oven at 50 °C for at least 24 h till constant sample weight.

Samples for SAXS study were prepared by pressing the blends between two pieces of Teflon films on a Linkam HFS91 hot stage at 190 ± 0.2 °C for 1 min. The samples were subsequently were directly transferred into an oven equilibrated at the temperature of 70 °C to allow the crystallization of PHB or P(HB-*co*-10% HV) for 4 days. Optical microscopy confirmed that volume-filling spherulitic were obtained through such a crystallization condition.

2.2. SAXS measurement

The SAXS experiments were conducted at the Department of Engineering and System Science, National Tsing Hua University, Taiwan. The power of X-ray source was operated at 200 mA and 40 kV. The X-ray source is an 18 kW rotating anode X-ray generator (Rigaku) equipped with a rotating anode Cu target. The incident X-ray beam was monochromated by pyrolytic graphite and a set of three pinhole inherent collimators was used so that the smearing effects inherent in slit-collimated small angle X-ray cameras could be avoided. The sizes of the first and second pinholes were 1.5 and 1.0 mm, respectively, and the size of the guard pinhole before the sample was 2.0 mm. The scattered intensity was detected by a two-dimensional position sensitive detector (ORDELA Model 2201X, Oak Ridge Detector laboratory Inc., USA) with 256×256 channels (active area 20×20 cm^2 with ~ 1 mm resolution). The beam stop was a round lead disc 18 mm in diameter. All data were corrected by the background (dark current and empty beam scattering) and the sensitivity of each pixel of the area detector. The area scattering pattern was radially averaged to increase the efficiency of data collection compared with a one-dimensional linear detector. Data were acquired and processed on an IBM compatible personal computer. The intensity profile was outputted as the plot of the scattering intensity (I) versus the scattering vector, $q = 4\pi/\lambda \sin(\theta/2)$, where θ is the scattering angle and λ is the X-ray wavelength.

2.3. Bulk crystallinity measurements

Bulk crystallinities of crystalline PHB/PVAc and P(HB-*co*-10% HV)/PVAc blends were calculated from the enthalpy of melting (Δh_f). The sample used for Δh_f measurement was cut directly from the specimens for SAXS measurement. The enthalpy of melting was measured by a TA Instrument 2000 differential scanning calorimeter (DSC). The bulk crystallinity (ϕ_c) was calculated by taking 146 J/g as the enthalpy of melting of 100% crystalline PHB [5], i.e. $\phi_c = \Delta h_f/146$.

3. Results and discussion

The lamellar microstructure of a crystalline/amorphous polymer blend can conveniently be probed from the profile of scattering intensity ($I(q)$) with scattering vector (q)

through the SAXS measurement. In the present study, we utilized the SAXS technique to probe and compare the lamellar morphologies of PHB/PVAc and P(HB-*co*-10% HV)/PVAc blends crystallized at 70 °C. Fig. 1 depicts the Lorentz-corrected SAXS profiles of PHB/PVAc and P(HB-*co*-10% HV)/PVAc blends. Crystallized PHB and P(HB-*co*-10% HV), both exhibited a typical scattering peak (q_{max}) associated with the electron density contrast between the alternating crystalline and amorphous layers. The position of q_{max} of both crystallized PHB and P(HB-*co*-10% HV) appear to be identical while the scattering intensity of the crystallized P(HB-*co*-10% HV) was slightly weak. This means that the existence of HV units did not affect the value of long period (L^{Bragg}) calculated by Bragg's law (i.e. $L^{Bragg}=2\pi/q_{max}$) but may be lowered the electron density difference between crystalline and amorphous layers for crystallized P(HB-*co*-10% HV). For the other blend compositions studied, the q_{max} peak associated with an existence of an alternating crystalline and amorphous layer stacking was also observed on the SAXS profile in Fig. 1. As can be seen in Fig. 1(a), the q_{max} in PHB/PVAc blends

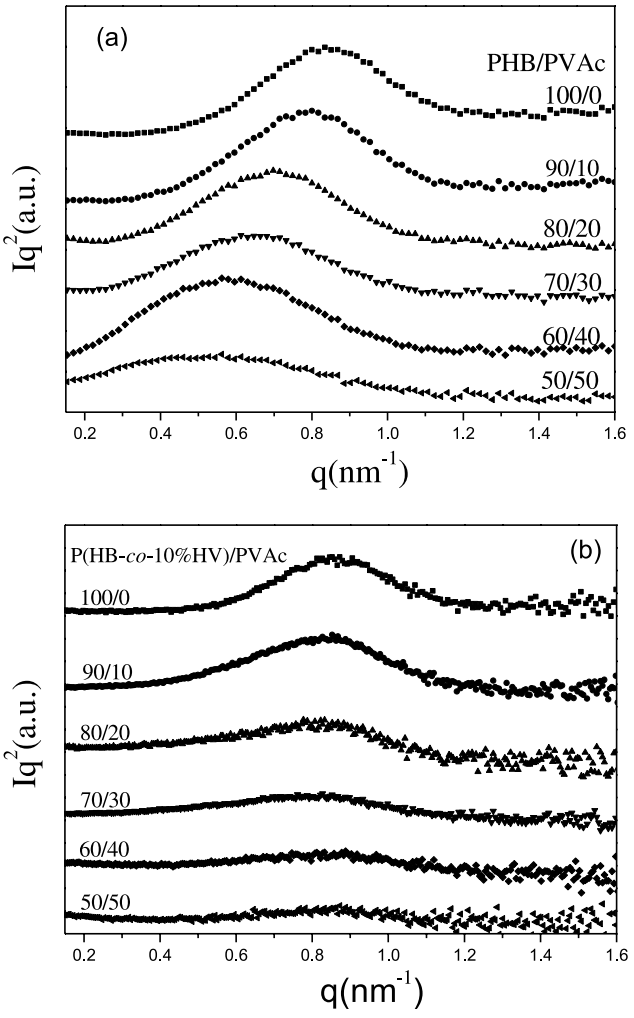

Fig. 1. Lorentz-corrected SAXS profiles of PHB/PVAc and P(HB-*co*-10% HV)/PVAc blends crystallized at 70 °C.

significantly shifted toward low q position with increasing PVAc composition, implying the addition of PVAc would increase the long period upon blending. In contrast, for the P(HB-*co*-10% HV)/PVAc blends in Fig. 1(b), the q_{max} was relatively independent of PVAc composition while the width of q_{max} peak was found to be broaded with the addition of PVAc, implying that the long period did not increase but the distribution of lamellar layers could be increased upon blending.

The morphological parameters including the crystal thickness (l_c), amorphous layer thickness (l_a), and the long period ($L=l_c+l_a$) may be evaluated by the one-dimensional correlation function ($\gamma(z)$) [18] defined to:

$$\gamma(z)=\frac{1}{Q}\int_0^\infty q^2 I(q)\cos(qz)\mathrm{d}q \tag{1}$$

where z is the direction along which the electron density is measured. Q is the scattering invariant.

$$Q=\int_0^\infty I(q)q^2\mathrm{d}q \tag{2}$$

Since, the experimentally accessible q range is finite, extrapolation of intensity to both low and high q is necessary for the integrations. Extrapolation to zero as accomplished by the Debye–Bueche model [19]

$$I(q)=\frac{A}{(1+a_c^2q^2)^2} \tag{3}$$

where A is a constant and a_c is the correlation length. A and a_c can be determined from the plot of $I(q)^{-0.5}$ versus q^2 using the intensity data at low q region. Extension to large q can be performed using the Porod–Ruland model [20–23]

$$I(q)=K_p\frac{\exp(-\sigma^2q^2)}{q^4}+I_{fl} \tag{4}$$

where K_p is the Porod constant, σ is a parameter related to the thickness of interphase between crystal and amorphous layers, and I_{fl} is the background intensity arising from thermal density fluctuation. The values K_p, σ, and I_{fl} were obtained by curve fitting the intensity profile at high q region. Fig. 2 represents the one-dimensional correlation functions of PHB/PVAc and P(HB-*co*-10% HV)/PVAc blends. Assuming the corresponding two-phase model, l_c, l_a, the most probable value of L can be estimated via simple geometric analysis of $\gamma(z)$, as demonstrated in Fig. 3. The thickness of the thinner layers (l_1) is given by the intersection between the straight line extended from the self-correlation triangle and the baseline given by $-A$. The average thickness of the thicker layer is then obtained from $l_2=L-l_1$. The assignment of l_1 and l_2 is governed by the magnitude of the linear crystallinity (ϕ_c^{lin}). When $\phi_c^{lin}<0.5$, the crystals contribute the smaller thickness; then $l_1=l_c$ and $l_2=l_a$. The inverse is true for $\phi_c^{lin}>0.5$. Linear crystallinity is defined as

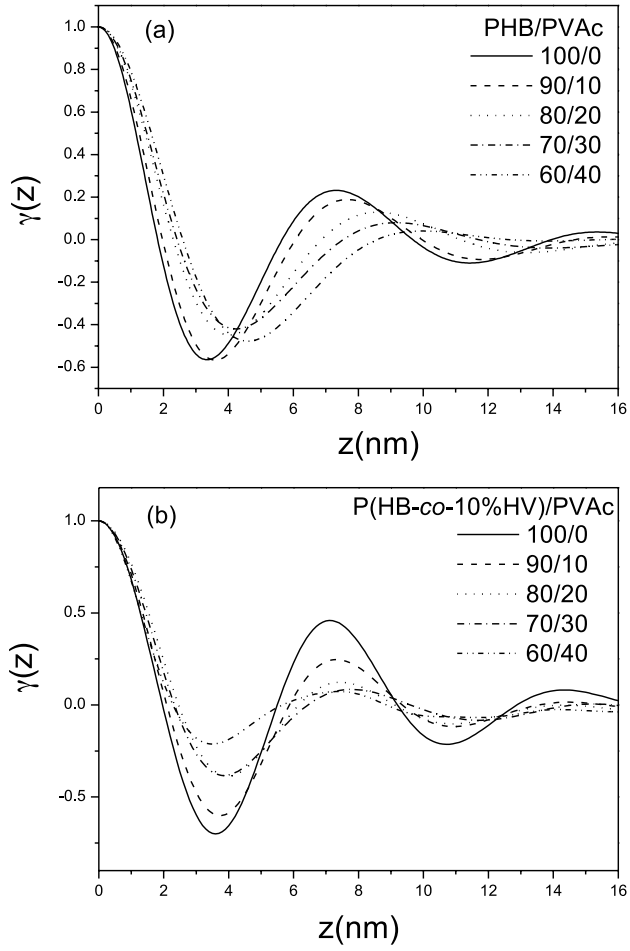

Fig. 2. One-dimensional correlation functions of PHB/PVAc and P(HB-*co*-10% HV)/PVAc blends crystallized at 70 °C.

$$\phi_c^{lin} = \frac{l_c}{L} = \frac{l_c}{l_c + l_a} \tag{5}$$

Provided that spherulites are volume filling, ϕ_c^{lin} is related to the bulk crystallinity, ϕ_c, by

$$\phi_c = \phi_s \phi_c^{lin} \tag{6}$$

where $\phi_s = \phi_c/\phi_c^{lin}$, the volume fraction of lamellar stacks in the sample. Since $\phi_s < 1$, Eq. (6) prescribes that the bulk crystallinity cannot be higher than the linear crystallinity. As a result, the assignment of l_1 and l_2 would be rather straightforward if the bulk crystallinity is greater then 0.5, because in this case the larger length, l_2, must correspond to the crystal thickness and l_1 to the amorphous layer thickness. In the present study, the ϕ_c lie above 50% for the majority of blend compositions investigated for both PHB/PVAc and P(HB-*co*-10% HV)/PVAc blends as shown in Fig. 4, so the l_1 and l_2 were assigned as l_a and l_c, respectively, as shown in Fig. 3.

Consequently, the values of ϕ_c^{lin} and ϕ_s could be obtained by Eqs. (5) and (6) as depicted in Figs. 4 and 5, respectively. Fig. 4 indicates the variations of ϕ_c and ϕ_c^{lin} with the weight fraction of PVAc (w_{PVAc}). The linear crystallinity, ϕ_c^{lin} (i.e. $\phi_c^{lin} = l_c/L$) is the crystallinity within lamellar stack, which is a local crystallinity. However, the bulk crystallinity, ϕ_c represents the crystallinity of the whole sample, which can be measured by DSC as described in Experimental section.

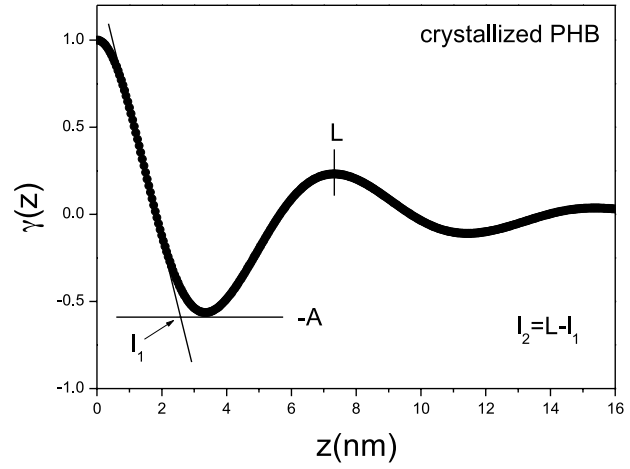

Fig. 3. l_c, l_a, the most probable value of L can be estimated via simple geometric analysis of $\gamma(z)$ (the thinner length, l_1, has been assigned to be l_a and the larger length, l_2, to be l_c).

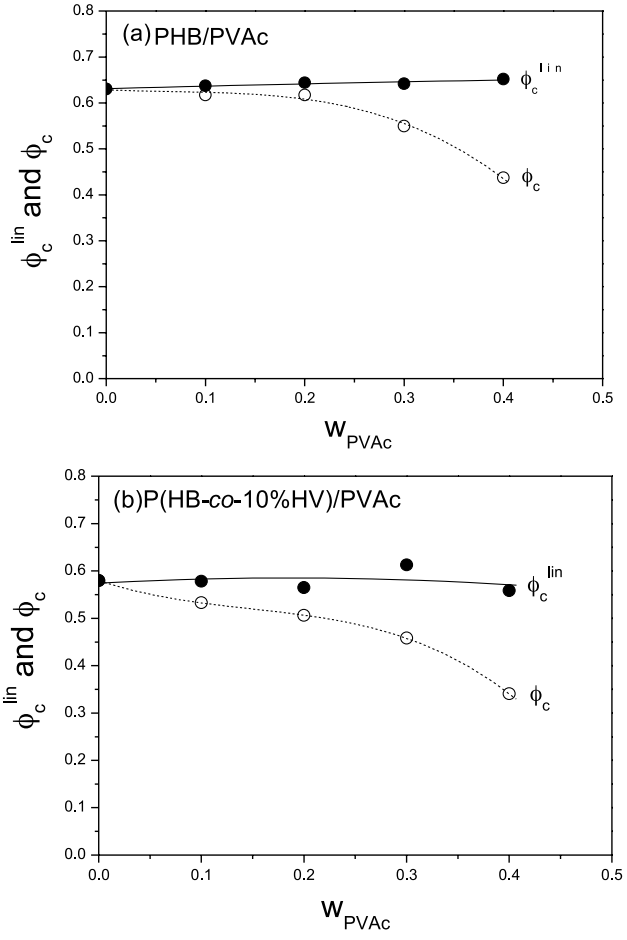

Fig. 4. Variation of ϕ_c and ϕ_c^{lin} with the weight fraction of PVAc; (a) PHB/PVAc blends; (b) P(HB-*co*-10% HV)/PVAc blends.

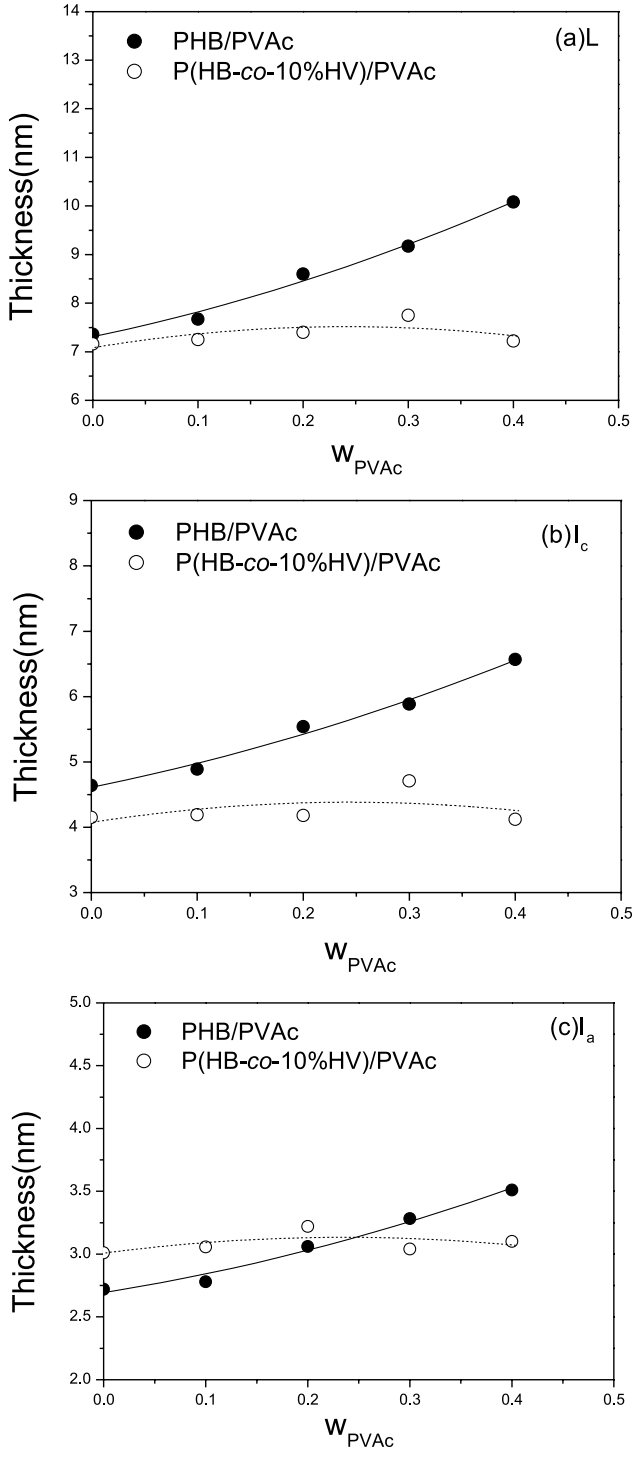

Fig. 5. Variations of L, l_c, and l_a as a function of w_{PVAc}.

If $\phi_c = \phi_c^{lin}$, the whole sample is homogeneously filled with lamellar stacks. Whereas, If $\phi_c < \phi_c^{lin}$, some space in the sample is not filled with lamellar stacks. In Fig. 4 for both PHB/PVAc and P(HB-*co*-10% HV)/PVAc blends, the value of ϕ_c^{lin} almost maintained constant with the addition of PVAc. However, it is observed that the composition variation of ϕ_c for PHB/PVAc blends less decreased as $w_{PVAc} \leqslant 0.2$ and then obviously decreased as $w_{PVAc} > 0.2$ but the trend of ϕ_c for P(HB-*co*-10% HV)/PVAc blends monotonically decreased with increasing PVAc composition. The both crystallinity quantities could clearly demonstrate the presence of interfibrillar segregation and indicate that the segregation morphology between PHB/PVAc and P(HB-*co*-10% HV)/PVAc blends is different. This discrepancy would be further illustrated as later section. Besides, it is also noticed that the ϕ_c or ϕ_c^{lin} values of crystallized P(HB-*co*-10% HV) were slightly less than those of crystallized PHB. This could be attributed to the isomorphous behavior due to the co-crystallization of HB and HV units in the co-polymer of P(HB-*co*-10% HV). Orts et al. have reported [24] that the HV units resided as defects within the crystal of the HB lattice and can be accommodated within the crystal lattice for such a co-polymer composition.

Fig. 5 shows the variations of L, l_c, and l_a with PVAc composition. It is observed that the values of L, l_c, and l_a for crystallized PHB were quiet approximate that reported by Canetti et al. [25] and those of crystallized P(HB-*co*-10% HV) were similar to the result reported by Rule et al. [26]. Compared with crystallized PHB, the crystallized P(HB-*co*-10% HV) has a larger l_a, a smaller l_c and L, implying the presence of the HV units in P(HB-*co*-10% HV) co-polymer limited, or constrained the thickness of crystalline lamellae. This is consistent with the postulate of the sandwich lamellae model proposed by Yoshie et al. [13]. They suggested that in P(HB-*co*-HV) of low HV content (i.e. $\leq$10 mol% HV) where the relatively long HB sequence are abundant and the entropy gain upon the co-crystallization is little, there must be marked tendency for the HV units to be excluded from the lamella, and the HV units may exist the lamella surface, where the distortion of the crystalline lattice upon the inclusion of the HV units can be easily relaxed.

More interesting, the values of L, l_c, and l_a in PHB/PVAc blends were found to be raise as the addition of PVAc, while those in P(HB-*co*-10% HV)/PVAc blends did not vary as the increase in PVAc composition. The trends of L, l_c, and l_a in P(HB-*co*-10% HV)/PVAc blends were similar to the results in P(HB-*co*-10% HV)/PMMA blends [17]. A comparison in L between PHB/PVAc and P(HB-*co*-10% HV)/PVAc blends is shown in Fig. 5(a), it is evident that the value of L in PHB/PVAc blends increased but in P(HB-*co*-10% HV)/PVAc blends did not vary with increasing w_{PVAc}. This trend of L in Fig. 5(a) was consistent with the observation of long period (L^{Bragg}) calculated by Bragg's law in Fig. 1.

In Fig. 5(b), the l_c in PHB/PVAc blends was seen to increase linearly with PVAc composition, implying the PHB crystals formed in the PHB/PVAc blends were thicker than those produced in the crystallized PHB. Whereas, l_c in P(HB-*co*-10% HV)/PVAc blends basically remained constant, indicating the thickness of P(HB-*co*-10% HV) crystals formed in the P(HB-*co*-10% HV)/PVAc blends did not be thickened by the presence of PVAc. This may be indicated that the structure of the isomorphous crystals of

P(HB-*co*-10% HV) in P(HB-*co*-10% HV)/PVAc blends was not affected by the addition of PVAc. The increase in l_c with increasing amorphous component has been observed such as poly(ethylene oxide) (PEO)/ethylene-methacrylic acid co-polymer [27], PEO/styrene-*p*-hydroxystyrene co-polymer [27] and polycaprolactone (PCL)/PVPh [28], attributed to the depression in equilibrium melting point (T_m^0), which lowers the degree of undercooling (i.e. $\Delta T = T_m^0 - T_c$) at a given T_c. According to the secondary nucleation theory [29,30], the initial crystal thickness is given by

$$l_g^* = \frac{2\sigma_e T_m^0}{\Delta h_f^0 (T_m^0 - T_c)} + \delta l \tag{7}$$

where σ_e is the fold surface free energy and Δh_f^0 is the bulk enthalpy of melting per volume.

At low to moderate degree of undercooling, δl is small, Eq. (7) thus reduces to

$$l_g^* \approx \frac{2\sigma T_m^0}{\Delta h_f^0 (T_m^0 - T_c)} \tag{8}$$

The final crystal thickness, according to the notation of Hoffman and Weeks [29,30], is γ times the initial thickness, i.e.

$$l_c = \gamma l_g^* \tag{9}$$

where γ is the so-called 'lamellar thickening factor'. Eq. (8) prescribes that the l_g^* is inversely proportional to the degree of undercooling. Because the decrease of T_m^0 upon blending lowers the degree of undercooling at a given T_c, the larger l_g^* may lead to the formation of thicker crystals in the blends. Due to the depression of T_m^0 in PHB/PVAc blends has been demonstrated in the prior study [31], it is suggested that the value of l_c in PHB/PVAc blends obviously increased with the addition of PVAc, which was mainly ascribing to the decrease in T_m^0. Above discussion concerning the increase in l_c has mainly focused on the consideration of crystallization thermodynamic. Nevertheless, the sizes of crystals may be also affected by the crystallization kinetic factor which may lead to the thickness of crystals does not increase with increasing amorphous component such as i-polystyrene (i-PS)/a-polystyrene (PS) [32] and i-PS/poly(propylene oxide) (PPO) [33] blends and so on. In the present study, owing to the co-polymer of P(HB-*co*-10% HV) containing 10 mol% HV unit, the presence of the ethyl side chain of HV units strongly affected the crystallization kinetics of HB units and the lattice or lamellar morphology was disturbed. Therefore, in Fig. 5(b), the l_c in P(HB-*co*-10% HV)/PVAc blends did not increase with increasing PVAc may be also considered due to both the crystallization kinetics and morphological factors resulted.

The effect of PVAc composition on the thickness of the amorphous layers is shown in Fig. 5(c). It is of interest that with increasing w_{PVAc}, l_a in PHB/PVAc blends was fund to be increased monotonically, while l_a in P(HB-*co*-10% HV)/PVAc blends did not vary. Again, this trend essentially indicates that the segregation morphologies in PHB/PVAc and P(HB-*co*-10% HV)/PVAc blends were quite different. For PCL/poly(vinyl chloride) (PVC) [1] and poly(vinylidene fluoride) (PVDF)/PMMA [27] blends, l_a monotonically increased with increasing amorphous component, which was mainly suggested to be the interlamellar segregation morphology. Therefore, the increase on l_a in PHB/PVAc blends was also suggested that the PVAc was mainly segregated into the PHB interlamellar regions during the PHB crystallization. For i-PS/a-PS [32] blends, both l_a and l_c were unaffected with the addition of a-PS but could were observed the volume-filling spherultes, and the bulk crystallinity decreased with the addition of a-PS, which was attributed to the interfibrillar segregation morphology. In this study, the observed composition variation of l_c and l_a in Fig. 5(b) and (c) for P(HB-*co*-10% HV)/PVAc blends were in good agreement with the results reported in i-PS/a-PS [32], therefore, it is suggested that amorphous PVAc was mainly segregated into the P(HB-*co*-10% HV) interfibrillar regions during the P(HB-*co*-10% HV) crystallization. Consequently, it could be conclude from the observation of l_a in Fig. 5(c) that the PHB/PVAc blends have mainly created the interlamellar segregation morphology, while P(HB-*co*-10% HV)/PVAc blends yielded the interfibrillar segregation morphology. On other words, the segregation distance of PVAc in P(HB-*co*-10% HV)/PVAc blends was greater than in PHB/PVAc blends. It is noticed that the segregation morphology of P(HB-*co*-10% HV)/PVAc blends was also similar to that of P(HB-*co*-10% HV)/PMMA blends, where l_a, and L were almost unaffected by the addition of PMMA [17].

The extent of interfibrillar segregation can also be determined from the magnitude of the volume fraction of lamellar stacks (e.g. the value of ϕ_s). The magnitude of ϕ_s is closely connected with the morphological structure. In the case of complete interlamellar segregation, the whole sample is homogeneously filled with lamellar stacks, so $\phi_s = 1$. A smaller ϕ_s implies a larger extent of interfibrillar segregation [28,34–37]. Fig. 6 plots the variation of ϕ_s as a function of w_{PVAc}. The ϕ_s values in P(HB-*co*-10% HV)/PVAc blends were basically lower than those of PHB/PVAc blends. This illustrates that the distance of PVAc segregation in P(HB-*co*-10% HV)/PVAc blends was greater than in PHB/PVAc blends. For PHB/PVAc blends, ϕ_s remained essentially constant at approximately unity when $w_{PVAc} \leq 0.2$, meaning that the morphological structure in this composition range is predominantly characterized by the interlamellar segregation. Above 20 wt% PVAc composition, ϕ_s dropped obviously with PVAc composition, indicating that interlamellar and interfibrillar segregation coexisted, and the extent of interfibrillar segregation increased with increasing of PVAc composition. However, for P(HB-*co*-10% HV)/PVAc blends, it is noticed that ϕ_s decreased monotonically with increasing PVAc composition, implying the morphological structure is

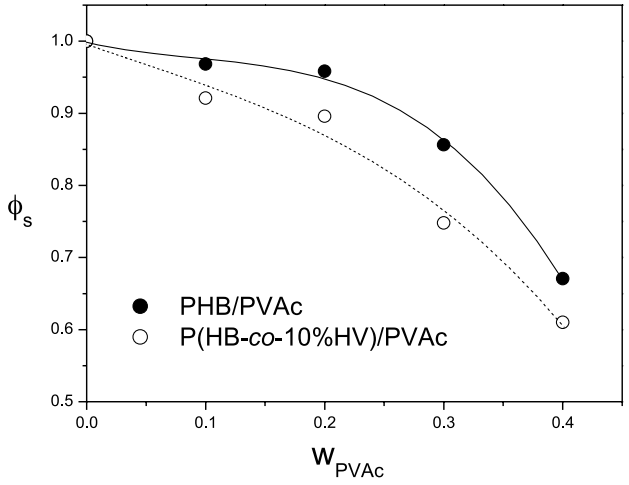

Fig. 6. Variation of ϕ_s as a function of w_{PVAc}.

predominantly characterized by the interfibrillar segregation, and the extent of interfibrillar segregation was also increased with the increase of PVAc composition. Since ϕ_s in P(HB-*co*-10% HV)/PVAc blends had a larger decrease, indicating the extent of extralamellar in P(HB-*co*-10% HV)/PVAc blends was enhanced. This may be suggested that the existence of HV in P(HB-*co*-10% HV) caused a depression of crystal growth rate and hence promoted the segregation distance of PVAc as described next section.

The segregation morphology for both PHB/PVAc and P(HB-*co*-10% HV)/PVAc blends may be understood in terms of the parameter δ defined by Keith and Padden [38] as $\delta = D/G$, where D is the diffusion co-efficient and G is the crystal growth rate. δ has the unit of length and thus provides a qualitative measure of segregation distance. Keith and Padden [38] suggested that the distance over which uncrystallizable impurity may be segregated is determined by the interplay between diffusion rate of impurity molecules and crystal growth rate. If the diffusion rate of diluent is relative slower than the crystal growth rate, diluent molecules may be trapped inside the interlamellar regions before they had a chance to diffuse out. In the present study, crystal growth rate was proposed to dominate the segregation distance of PVAc. The extent of interfibrillar segregation in P(HB-*co*-10% HV)/PVAc blends was greater than PHB/PVAc blends, attributed to crystal growth rate is the dominant factor in controlling the segregation distance of PVAc due to the extremely slower crystal growth rate of P(HB-*co*-10% HV) [13,39,40]. Furthermore, increasing PVAc composition induced a stronger depression in growth rate and consequently promoted the extent of interfibrillar segregation for both PHB/PVAc and P(HB-*co*-10% HV)/PVAc blends.

On the basis of the composition variation of l_a, and the magnitude of ϕ_s, it is affirmatively established that the segregation distance of PVAc was promoted by increasing PVAc composition for both PHB/PVAc and P(HB-*co*-10% HV)/PVAc blends. In addition, the segregation of PVAc in P(HB-*co*-10% HV)/PVAc blends was more easily than in PHB/PVAc. These consequences can be interpreted by the postulate that crystal growth rate is the dominant factor to control the segregation distance of the amorphous diluent, slower growth rate may result in a larger extent of extralamellar segregation, since the amorphous diluent can diffuse out more easily and avoids being trapped in side the interlamellar regions.

4. Conclusion

The segregation morphology of PHB/PVAc and P(HB-*co*-10% HV)/PVAc blends have been investigated by SAXS. Blending with PVAc thickened the PHB crystals but not the P(HB-*co*-10% HV) crystals. On the basis of the composition variation of l_a, and the magnitude of ϕ_s, it is affirmatively established that the distance of PVAc segregation was promoted by increasing PVAc composition for both PHB/PVAc and P(HB-*co*-10% HV)/PVAc blends. In addition, the segregation of PVAc in P(HB-*co*-10% HV)/PVAc blends was more easily than in PHB/PVAc. For PHB/PVAc blends, the morphological structure is predominantly characterized by the interlamellar segregation when $w_{PVAc} \leq 0.2$ and the interlamellar and interfibrillar segregation coexisted above 20 wt% PVAc composition. For P(HB-*co*-10% HV)/PVAc blends, the morphological structure is predominantly characterized by the interfibrillar segregation. These consequences can be interpreted by the postulate that crystal growth rate is the dominant factor to control the segregation distance of the amorphous diluent, slower growth rate may result in a larger extent of extralamellar segregation, since the amorphous diluent can diffuse out more easily and avoids being trapped inside the interlamellar regions.

Acknowledgements

We are grateful for the support of SAXS beamtime from Prof Tsang-Lang Lin at the Department of Engineering and System Science, National Tsing Hua University, Taiwan. This work was supported by the National Science Council, ROC, under Grant NSC 92-2216-E-233-001.

References

[1] Stein RS, Khambatta FB, Warner FP, Russell T, Escala A, Balize E. J Polym Sci Polym Symp 1978;63:313.
[2] Lemoigne M. Ann Inst Past 1925;39:144.
[3] Dawes EA, Senior PJ. Adv Microbiol Physiol 1973;10:330.
[4] Findlay RH, White PC. Appl Environ Micron Microbiol 1983;45:71.
[5] Barham PJ, Keller A, Otun EL, Holmes P. J Mater Sci 1984;19:2781.
[6] Doi Y. Microbiology polyester. New York: VCH Publishers Inc.; 1990.
[7] Mitomo H, Barham PJ, Kell er A. Polymer J 1987;19:1241.

[8] Holmes PA. In: Bassett DC, editor. Developments in crystalline polymers-2. Amsterdam: Elsevier; 1988.
[9] Bluhm TL, Hamer GK, Marchessault RH, Fyfe CA, Veregin RP. Macromolecules 1986;19:2871.
[10] Kunioka M, Tamaki A, Doi Y. Macromolecules 1989;22:694.
[11] Scandola M, Ceccorulli G, Pizzoli M, Gazzano M. Macromolecules 1992;25:1405.
[12] Yamada S, Wang L, Asakawa N, Yoshie N, Inoue Y. Macromolecules 2001;34:4659.
[13] Yoshie N, Saito M, Inoue Y. Macromolecules 2001;34:8953.
[14] Canetti M, Sadocco P, Sicilliano A, Seves A. Polymer 1994;35:2884.
[15] Chiu HJ, Chen HL, Lin TL, Lin JS. Macromolecules 1999;32:4969.
[16] Chiu HJ. J Appl Polym Sci 2004;92:3595.
[17] Chiu HJ, Shu WJ. Accepted for publication.
[18] Strobl GR, Schneider M. J Polym Sci, Polym Phys Ed 1980;18:1343.
[19] Debye P, Bueche AM. J Appl Phys 1949;20:518.
[20] Ruland WJ. J Appl Crystallogr 1971;4:70.
[21] Porod G. Kolloidn Zh 1951;124:83.
[22] Porod G. Kolloidn Zh 1952;125:51.
[23] Porod G. Kolloidn Zh 1952;125:108.
[24] Orts WJ, Machessault RH, Bluhm TL. Macromolecules 1991;24:6435.
[25] Canetti M, Urso M, Sadocco P. Polymer 1999;40:2587.
[26] Rule RJ, Liggat JJ. Polymer 1995;36:3831.
[27] Talibuddin S, Wu L, Runt JP, Lin JS. Macromolecules 1996;29:7527.
[28] Chen HL, Wang SF, Lin TL. Macromolecules 1998;31:8924.
[29] Hoffman JD, Weeks JJ. J Res Natl Bur Stand A: Phys Chem 1962;66A:13.
[30] Hoffman JD, Miller RL. Polymer 1997;38:3351.
[31] Greco P, Martuscelli E. Polymer 1989;30:1475.
[32] Warner FP, Macknight WJ, Stein RS. J Polym Sci, Polym Phys Ed 1997;15:2113.
[33] Wenig W, Karase FE, Macknight WJ. J Appl Phys 1975;46:4194.
[34] Chen HL, Hsiao MS. Macromolecules 1998;31:6579.
[35] Chen HL, Li LJ, Lin TL. Macromolecules 1998;31:2255.
[36] Talibuddin S, Wu L, Runt J. Macromolecules 1996;29:7527.
[37] Wang C, Liao WP, Cheng YW, Lin TL. Polymer 2004;45:961.
[38] Keith HD, Padden FJ. J Appl Phys 1975;35:1270.
[39] You JW, Chiu HJ, Shu WJ, Don TM. J Polym React 2003;10:47.
[40] Yoshie N, Fujiwara M, Ohmori M, Inoue Y. Polymer 2001;42:8557.